The DOI for this manuscript is doi: 10.1175/JTECH-D-17-0079.1

Schmidt, K., S. Swart, C. Reason, and S. Nicholson, 2017: Evaluation of satellite and reanalysis wind products with in situ Wave Glider wind observations in the Southern Ocean. J. Atmos. Oceanic Technol. doi:10.1175/JTECH-D-17-0079.1, in press.

Evaluation of satellite and reanalysis wind products with *in situ* Wave Glider wind observations in the Southern Ocean

Kevin M. Schmidt[a], Sebastiaan Swart[b,c,d], Chris Reason[c], Sarah Nicholson[b,c]

[a] *Marine Research Institute, University of Cape Town, Rondebosch, South Africa*

[b] *Southern Ocean Carbon & Climate Observatory, Council for Scientific and Industrial Research, Rosebank, South Africa*

[c] *Department of Oceanography, University of Cape Town, Rondebosch, South Africa*

[d] *Present address: Department of Marine Sciences, University of Gothenburg, Gothenburg, Sweden*

Corresponding author email:

Sebastiaan Swart: sebastiaan.swart@marine.gu.se

Keywords: Sea surface winds, reanalysis, intercomparison, wave gliders, wind speed, scatterometer, wind products, Southern Ocean

Abstract

Surface ocean wind datasets are required to be of high spatial and temporal resolution and high precision to accurately force or be assimilated into coupled atmosphere-ocean numerical models and understand ocean-atmospheric processes. *In situ* observed sea surface winds from the Southern Ocean are scarce and consequently the validity of simulation models is often questionable. Multiple wind data products were compared to the first known high resolution *in situ* measurements of wind speed from Wave Glider (WG) deployments in the Southern Ocean with the intent to determine which blended satellite or reanalysis product best represents the magnitude and variability of the observed wind field. Results show that the ECMWF reanalysis product is the most accurate in representing the temporal variability of winds, exhibiting consistently higher correlation coefficients with *in situ* data across all wind speed categories. However, the NCEP-DOE AMIP Reanalysis-2 product matches *in situ* trends of deviation from the mean and performs best in depicting the mean wind state, especially during high wind states. The ECMWF product also leads to smaller differences in wind speeds from the *in situ* data, while CFSv2 showed slightly higher biases and a greater RMSE. The SW product consistently performed poorly at representing the mean or wind stress variability compared to those observed by the WG. Overall, the study shows autonomous surface vehicles provide valuable observations by which to validate, understand and potentially assist in correcting satellite/reanalysis products, particularly in remote regions, where few *in situ* estimates exist.

1. Introduction

Mid- to high-latitude regions in the Southern Ocean are host to the strongest wind fields at the ocean surface. These strong winds (e.g. speeds >20 m s^{-1}; Yuan (2004)) significantly impact upper ocean properties and processes, such as mixed layer dynamics, Ekman processes and air-sea exchange. Exchanges in heat, moisture, and momentum at the air-sea interface are facilitated by sea surface winds. In addition to driving physical processes at the sea surface, these winds also have implications for biological processes which extend below the surface. The flux of carbon dioxide (CO_2) between the atmosphere and ocean is closely related to wind speed (Wanninkhof, 1992, 1999, 2009, Nightingale, 2000, Ho et al., 2006), and as such, sea surface winds are of interest to many scientists studying and modeling biogeochemical cycles within the ocean.

Surface ocean winds are measured using *in situ* techniques or remote sensing instruments. Satellite instruments interpret variability in lidar laser energy reflection due to sea surface roughness to infer wind vectors generally at a height of 10 meters above sea level, while *in situ* measurements are generally taken at varying heights above sea level dependent on the platform (e.g. ship, mooring, or glider). Due to the varying methods of collecting and synthesizing wind measurements, the uniformity of sea surface wind data is often questioned. Such inconsistencies require studies reliant on satellite derived wind data (such as Yuan et al., 2009) to perform a validation prior to the start of their analysis in order to determine the ability of satellite blended datasets to accurately represent wind fields at the air-sea interface, and to see if post processing is required to reduce errors once compared to *in situ* measurements. There is a great need to reduce or eliminate this time costly step in wind data analysis. Further, the dearth of *in situ* wind stress observations in the Southern Ocean, particularly in winter (practically

absent – Gille et al., 2016), is resulting in poorly constrained ocean and climate models, where wind forcing is reliant on un-validated scatterometer or reanalysis wind products. This particular problem, together with air-sea flux uncertainties in general, were highlighted at a recent international workshop that brought together scientists to discuss this issue and how it could be addressed (Gille et al., 2016). Through the Southern Ocean Observing System (SOOS) a new capability working group has been formed on enhancing parameterizations of air-sea fluxes in the Southern Ocean. It is hoped this will attempt to address, discuss and engage with the larger community on the severe lack of flux observations and the associated research issues emanating from this (http://soos.aq/activities/capability-wgs/soflux).

Several studies have made attempts to compare and validate wind products in the Southern Ocean. Yuan (2004), Yuan et al. (2009), and Patoux (2009) highlight the implications of misrepresented wind fields in the Southern Ocean in their evaluations of extreme wind events in the Southern Ocean. Yuan (2004) compared Quick Scatterometer (QuikSCAT) wind data with reanalysis wind data from the National Centers for Environmental Prediction (NCEP), National Center for Atmospheric Research (NCAR) and European Centre for Medium-Range Weather Forecasts (ECMWF). This study showed that both weather station and QuikSCAT winds were stronger than reanalysis data, albeit only during high wind events. Their approach required the input of many different wind products to investigate the spatial and seasonal variability of high wind characteristics. Due to the remote area of the study, the reanalysis products that they used were limited with regard to *in-situ* data input. It was shown that monthly mean wind observations from satellite averages over the Southern Ocean were in agreement with model simulations except for the period from May to October (6 months centered over austral winter), when scatterometer winds were stronger than simulated winds, thereby suggesting a strong winter bias

in data. Similar to Hilburn et al. (2003), Yuan (2004) attributed this discrepancy to the NCEP/NCAR reanalysis missing some storms entirely, along with a lack of observational data assimilated into the reanalyses. Additionally, Yuan et al. (2009) further investigated a study by Patoux et al. (2009), where scatterometer derived pressure fields were modified using reanalysis wind data. QuikSCAT data were blended with ECMWF forecast data to produce modified pressure swaths. Yuan et al. (2009) claim that even small mesoscale cyclones contribute significantly to heat and momentum fluxes at the air-sea interface due to the high frequency of their occurrence. As such, a correct representation of mesoscale cyclones in numerical weather prediction (NWP) models of the Southern Ocean is therefore critical (Yuan et al. 2009). Although these studies have aided in improving estimates of wind stress and understanding time and space variability of Southern Ocean wind events, significant gaps in our understanding of wind stress accuracy and uncertainty remain. For instance, at any given location the diurnal variability of wind stress is often subject to aliasing due to the geographical variability of sampling by satellite, and the higher harmonics of the fundamental diurnal cycle may be distorted or eliminated (Risien and Chelton, 2008). New acquisitions of *in situ* data from robotic platform deployments, such as presented in this study, are likely to play an ever increasing role in understanding wind stress (and other air-sea fluxes) characteristics and validating gridded wind stress products, especially in remote and harsh locations of the worlds ocean where historically field data has a strong bias to the summer season (Gille et al., 2016).

The aim of this paper is to determine which wind data product (satellite blended, reanalysis and modelled) best represents the *in situ* wind field magnitude and variability of a study location in the Subantarctic Southern Ocean. This is done by comparing wind products with a valuable set of time series of *in situ* sea surface wind data collected by Wave Glider (WG)

technology deployed in a series of experiments in the Southern Ocean. The paper is organized as follows: an explanation of the surface wind datasets, their sources, and the transformations performed to collocate them in space and time. In the following section, a detailed description of the statistical analysis performed in this study is provided, while in Section 3, remotely measured winds are compared with *in-situ* winds at a quasi-fixed location in the Southern Ocean. The final section presents a discussion of the results and their broader implications for other scientific disciplines.

2. Data and methodology

2.1 In situ wind observations and experimental setup

The *in-situ* data used in this study were collected via a Liquid Robotics Wave Glider (WG) autonomous surface vehicle. The primary components of the WG include a surface float, a subsurface unit, and a 7-meter-long umbilical cable, which connects the two (Figure 1). The fins installed on the subsurface unit convert orbital motion of surface waves into horizontal force that drives the subsurface unit forward. The subsurface unit tows the surface float at speeds ranging between 0.5-2 knots. Solar panels and batteries power sensors and communication systems that are installed in the surface float, enabling it to remain at sea for an extended period of time (multiple months). The experiment was located in the domain of austral summer maximum wind speed (December 2015 average > 10 m s^{-1}), associated with the westerly winds of the Southern Ocean, as indicated by the red shading band in Figure 1(a). Two different Wave Glider deployments took place in the austral winter to summer of 2015. Gliders ‘CSIR2’ and ‘CSIR1’ were deployed in July and November of 2015, respectively, and were set to navigate to 43°S,

8.5°E. Upon arrival at the study site a pseudo-mooring octagon sampling pattern (Figure 2) with a diameter of 16 km was maintained (further details in Monteiro et al., 2015). At the center of the octagon, a Seaglider profiled the upper 1km of the ocean in pseudo-mooring mode.

The WG is designed to augment existing marine technology by providing autonomous real-time data collection of parameters near the air-sea interface. The Council for Scientific and Industrial Research (CSIR) uses this technology in their integrated multi-platform approach for a series of the Southern Ocean Seasonal Cycle Experiments (SOSCEx), which use research vessels, WGs, profiling gliders, bio-optic floats, satellite data and numerical models to explore the climate sensitivity of carbon and ecosystem dynamics (Swart et al., 2012). The WGs deployed during the research expeditions were equipped with an Airmar WX-200 Ultrasonic Weatherstation Instrument (more at www.airmar.com/uploads/brochures/WX-OFFSHORE.pdf). This instrument is a compact weather station designed for moving platforms, with abilities to dynamically correct winds using an internal compass and correct up to 30° pitch in rough seas. The sensor outputs apparent and true wind speed and direction (via ultrasonic transducers that are able to measure wind speed readings up to 40 m s^{-1}), barometric pressure, air temperature, and GPS location. The meteorological sensor was mounted on a mast attached to the surface float of the WG at 0.70 m above sea level. The sensor sampled at 1 Hz and then averaged over 10 minute bins before transmitting data back to shore via Iridium satellite communications.

As stated by the manufacturer, the sensor has the following wind speed measurement accuracies depending on wind speed categories: 0-5 m s^{-1}: 0.5 m s^{-1} RMS; 5-40 m s^{-1}: 1 m s^{-1} RMS. In wet conditions, which include rain, frost, snow or severe sea spray, errors may increase to 2.5 m s^{-1} due to moisture flow through the wind channel. This is expected to have a reduced

impact on the data accuracy due to the bin averaging in the field as well as in relating the *in situ* wind speed with longer term 6 hourly satellite or reanalysis wind products.

2.2 Satellite/reanalysis wind data

The SeaWind (SW) globally gridded and blended sea surface vector winds were generated from the multiple satellite observations of DOD, NOAA and NASA along with the input of satellite wind retrievals from Remote Sensing Systems, Inc. More information about the satellites, instruments, and blending scheme can be found at https://www.ncdc.noaa.gov/data-access/marineocean-data/blended-global/blended-sea-winds. The methods used to generate such data include objective analysis and simple spatiotemporally weighted interpolation. This product provides global ocean coverage with a spatial resolution of 0.25° x 0.25° and a 6 hourly temporal resolution. The data are provided at 10m above sea level.

NOAA uses a global NWP model called the Climate Forecast System which represents the interaction between the air-sea interfaces throughout the world's oceans. The CFS version II (CFSv2) operational near real time wind vector dataset provides time series at a period of record from 01 January 2011 – 01 April 2016 at a 6 hourly temporal resolution (Saha et al., 2014). CFS time series products are available at a spatial resolution of 0.205° x 0.204° at 10m above sea level.

European Centre for Medium-range Weather Forecasts (ECMWF) ERA-Interim Global Reanalysis Sea Surface Winds are provided at a spatial resolution of 0.125° x 0.125° (Dee et al., 2011). The project is in near real-time production and the data are calculated at 10m above sea level and are available at a 6 hourly temporal resolution.

Lastly, the NCEP/NCAR Reanalysis project has created a sea surface wind dataset which covers the period from 01 January 1979 to the present. Due to increasing user processing errors and systematic biases in NCEPI, the development of the NCEP–DOE AMIP-II Reanalysis (R-2), or NCEPII, was initiated in the late 1990's (Kanamitsu et al., 2002). NCEPII is of the same spatial (1.9047° x 1.8750°) and temporal resolution as NCEPI and incorporates similar raw observational data. The data are calculated at a height of 10m above sea level and are available at a 6 hourly temporal resolution.

2.3 Data comparison approaches

Satellite winds are derived from sea surface backscatter observed by microwave sensors in orbit to generate wind in an equivalent neutrally stable state. This estimation is based on the variation of normalized radar cross section as a function of local wind conditions and observation geometry (Freilich and Vanhoff, 2002). When a lidar laser beam hits a calm water surface at near normal incidence roughly 2% of the energy is reflected with little divergence; however, with increasing wind speed and subsequent surface roughening the divergence angle of the reflected energy increases and the intensity of lidar backscatter decreases (Yongxiang Hu, 2009). This process makes them sensitive to ocean surface roughness due to the stratification of the atmosphere above sea level. These sensors are thus calibrated to an equivalent neutral wind at a reference height of 10m above the sea surface (Liu and Tang, 1996; Bourassa et al. 1999a; Bourassa et al. 2003; Chelton et al. 2004). These equivalent neutral winds are the winds that would exist if the atmospheric boundary layer was neutrally stratified (Chelton et al. 2004; Carvalho et al. 2013). An observation operator (Tardif and Laroche, 2012B) is typically applied to vertically interpolate wind information through the surface layer to the specified 10m height

using the logarithmic wind profile and Monin- Obukov similarity functions (as described by Geleyn, 1988). Consequently, to compare real-time stability dependent winds to equivalent neutral winds, a transformation must be performed to shift the WG winds to the same reference level as satellite winds. Any extrapolation method to shift measured wind speed to a different height is a function of atmospheric turbulence. Wind shear and the buoyant forcing of the atmosphere must be taken into account; ultimately the vertical density stratification of the atmosphere must be accurately represented (Ruti et al., 2008).

Various methods have been used depending on the amount of input data available. One commonly used method, proposed by Liu and Tang (1996) is based on the bulk aerodynamic relation. This approach requires additional observational inputs of air and sea surface temperature (SST), relative humidity, and atmospheric pressure which are not available for this study period and site. As in Satheesan et al. (2007), Singh et al. (2013), Sudha and Rao (2013), and Yang et al. (2014), the present study required a method which does not include inputs associated with atmospheric stability. Bentamy et al. (2008) and Qing and Chen (2015) use the wind profile power law in their validation tasks of OSCAT and ASCAT wind data in the Atlantic Ocean. With this method, neutrally equivalent winds are calculated with the use of the coefficient (α) which varies with atmospheric stability. However, no intercomparison has been performed to determine the difference between a power expression method and the method proposed by Liu and Tang (1996). Therefore, the present study uses a mixing-length approach used by Herrera et al. (2005), Ruti et al. (2008), Carvalho et al. (2013), Singh et al. (2013), Alvarez et al. (2014) and Yang et al. (2014) in the vertical transformation of *in situ* surface wind data to a reference height of 10 meters. With no atmospheric stability input, a logarithmic method proposed by Peixoto and Oort (1992) is used. This is expressed as

$$U_Z = U_{Z_m} \frac{\ln\frac{Z}{Z_0}}{\ln\frac{Z_m}{Z_0}}, \quad (1)$$

where U_z is wind speed at height Z, Z_m denotes measurement height, and Z_0 represents the roughness length. A typical oceanic value of 1.52×10^{-4} m was assumed for Z_0 (Peixoto and Oort, 1992). This approach generates a logarithmically varying vertical wind profile while assuming neutral stability conditions. An inter-comparison of the correction methods proposed by Liu and Tang (1996) and by Peixoto and Oort (1992) was performed by Mears et al. (2001). They conducted a comprehensive analysis to determine if these laws can account for effects due to differences in atmospheric stability. It was concluded that the Liu and Tang (1996) correction is typically on average 0.12 m s^{-1} stronger than a logarithmic correction (Mears et al., 2001; Pickett et al., 2003; Ruti et al., 2008). Under stable conditions, Liu and Tang (1996) corrected winds are greater than logarithmic corrected winds, and for unstable conditions the opposite is seen (Carvalho et al., 2013). Ruti et al. (2008) also compared these correction methods and concluded that generally a difference in collocated wind speed is only observed during extreme wind events, where wind speeds exceed 15 m s^{-1}. Singh et al. (2013) conclude that during these extreme wind events, wind speed transformation carried out by a logarithmic profile may lead to errors of 1–1.5 m s^{-1}. However, it can be assumed that the use of a logarithmic extrapolation method will not cause discernable error as there are very few instances in the WG data where the wind speed is greater than 15 m s^{-1}.

An instantaneous sampling approach may be appropriate in cases where the *in-situ* time series matches exactly with the satellite time series. On the other hand, according to Ruti et al. (2008) an averaging method may require consideration of the phase velocities of cyclones in the region of interest. By determining the typical phase velocity for Mediterranean cyclones, they

242 could determine a general time frame of 30-60 minutes over which *in-situ* data from the
243 Mediterranean should be averaged when compared with scatterometer winds. Other studies,
244 such as one by Bourassa et al. (2003), state that the optimal averaging period varies with respect
245 to wind speed at the moment of observation. During high wind periods, a shorter averaging
246 period may result in a smaller RMSE, whereas during low wind speed periods, longer averaging
247 periods could also have the same effect . This variability in optimum averaging time with respect
248 to wind speed is anticipated from Taylor's hypothesis (Taylor, 1938). This study took an
249 averaged sampling approach to binning the time series. Data was transmitted back to the base
250 station in 10 minute averages. Each time series consisted of more than ten thousand wind
251 measurements. For analysis the data was binned twice, first to create an hourly product and then
252 a 6 hourly product. Instead of sampling over the duration of each hour, two data points before
253 and after each desired interval were averaged.

254 In order to compare blended wind fields from satellite data with the WG observations, a
255 collocation procedure was necessary to match the datasets spatially and temporally. For all wind
256 products, a linear interpolation procedure was performed to produce wind pairs from both
257 datasets. This method was possible due to the aforementioned temporal gridding of the WG data.
258 Because the WGs were set to circle a fixed point, the majority of the collocations were
259 performed on a coordinate points close to 43°00'S 8°30'E (Figure 2).

260 ***2.4 Statistical comparison***

261 WG meteorological records are provided every 10 minutes, while the satellite products
262 and numerical weather products provide four data points per day (corresponding to the hours
263 00H00, 06H00, 12H00, and 18H00 UTC). Initial statistical analysis is intended to assess the
264 quality of the simultaneous records with respect to temporal and spatial accuracy. In order to

265 determine if the error associated with the satellite and reanalysis derived wind data is related to a
266 particular wind speed, the wind data were analysed as a whole as well as in low, medium, and
267 high wind speed categories. The thresholds for these wind speed categories were determined by
268 the lower and upper quartiles of the WG dataset. This varied slightly for each time series; the
269 winter-spring deployment of the CSIR2 WG in 2015 had a low speed threshold of 7.3 m s^{-1}, and
270 a high speed threshold of 12.4 m s^{-1}, while during austral summer CSIR1 WG had a low speed
271 threshold of 9.0 m s^{-1}, and a high speed threshold of 16 m s^{-1}. The purpose of this approach was
272 to show the error dependence on wind speed as well as to determine which product best
273 represented each wind category.

274 The mean and the standard deviation of all wind products per wind speed category are
275 calculated with the intent to show the standard variance from the mean. Statistical parameters
276 such as the Root Mean Square Error (RMSE)and correlation coefficient (R^2) are calculated to
277 assess the ability of the wind products to represent the observed winds. U_i and U_j are variables
278 which represent the satellite product wind speed and the observed wind speed by the WG,
279 respectively. N is the total number of paired simulation/ observed records. More specifically,
280 these parameters will determine the accuracy of the varying wind product's ability to represent
281 the temporal variability of the wind. Bias is calculated to evaluate the tendency of the data and is
282 intended to estimate differences in the mean state of the wind field. The intent of observing this
283 parameter is to determine if wind products tend to over/underestimate the WG measured wind
284 speed.

285 Lastly, Weibull Probability Density Functions (PDF's) were used to evaluate the various
286 wind products ability to describe the WG measured wind regime. This method was similarly
287 used by Liu et al. (2008) and Carvalho et al. (2013) in their assessment of QuikSCAT and Cross-

Calibrated Multi-Platform (CCMP) surface winds ability to characterize buoy measured wind regimes closest to reality.

3. Results

Wind speeds measured by the WG are compared against the corresponding gridded 10m surface winds available from various products. Initially, comparison was made between the entireties of all datasets. After hourly and 6 hourly binning methods were applied, each WG deployment rendered the following number of data points in the 6-hourly bins to compare to 6-hourly wind products: CSIR2- 27 July 2015 to 02 November 2015: n = 394; CSIR1- 07 December 2015 to 07 February 2016: n = 252 (Figure 3).

In order to understand the degree of variance from the mean of each product, the mean and standard deviation of all wind products per wind speed category are provided in Table 2. The mean for the varying wind speed categories increases with respect to wind speed. Additionally, the magnitude of increase in the mean is fairly uniform between low and medium wind speeds (on average an increase of 2-3 m s^{-1}, except for both CSIR series which have an increase of ~5-6 m s^{-1}). However, this magnitude varies significantly between medium and high wind speed categories for all wind products. For instance, during both time series the differences in the medium and high wind means of the SW product increased on the order of 1-2 m s^{-1}, while the differences for other wind products were on the order of 5-7 m s^{-1}.

During the CSIR2 WG time series in 2015 the SW, ECMWF, and CFSv2 products underestimated the mean state by approximately 0.3 m s^{-1} while the NCEPII product overestimated the mean state by approximately 1.1 m s^{-1}. All wind products underestimated the mean state of the winds recorded by the CSIR1 WG by approximately 2.9 m s^{-1} in 2015-2016, although the underestimation of the NCEPII product was on average just 1.3 m s^{-1} less than the

311 *in situ* data. The variance of the mean of the WG data, as depicted by the standard deviation, is
312 consistent at low and medium wind speeds, and increases slightly (approximately 20% increase)
313 for high wind speeds. The only wind product which depicted this trend was NCEPII and during
314 both time series, this product's low wind speed category had a lower variance (averaged ±3.2 m
315 s^{-1}) with respect to the variance of the high wind speed category (averaged ±4.0 m s^{-1}). The SW
316 product exhibited low variance (averaged ±2.9 m s^{-1}) with low and high speeds, while the
317 greatest variance from the mean was at medium wind speeds (averaged ±3.2 m s^{-1}). The
318 ECMWF product consistently exhibited a trend of decreasing variance with an increase in wind
319 speed (averaged low wind variance ±2.6 m s^{-1} compared to averaged high wind variance of ±2.2
320 m s^{-1}). The CFSv2 product exhibited the most consistent variance across time series and wind
321 speed categories with an average variance of ±2.9 m s^{-1} for the CSIR2 time series, and an
322 average variance of ±2.3 m s^{-1} for the CSIR1 time series.

323 Further statistical comparison was conducted using root mean square error, mean bias,
324 and the correlation coefficient (Table 3). Globally, there is a tendency for satellite product wind
325 speed errors, as depicted by RMSE, to be greater in the presence of low and high winds
326 (Carvalho et al., 2013). This trend was especially apparent for the SW product during the CSIR2
327 time series. However, also during this time series the ECMWF, CFSv2, and NCEPII products
328 exhibited the highest RMSE for the low wind speed category. For the CSIR1 time series, the
329 SW, ECWMF, and CFSv2 products exhibited the opposite trend where the high wind speed
330 category had the highest RMSE. Only the NCEPII product exhibited the trend described by
331 Carvalho et al. (2013) during this time series. The ECMWF product exhibited the lowest RMSE
332 across all wind speed categories during the CSIR2 time series, whereas during the CSIR1 series

333 the NCEPII product had the lowest RMSE for the all, medium and high wind speed categories
334 (outperformed by CFSv2 and ECMWF for the low wind speed category).

335 The time series correlation using data collected by WG CSIR2 from July 2015 to
336 November 2015 (Figure 4) represents an extensive austral winter to spring dataset while the time
337 series collected by WG CSIR1 from December 2015 – February 2016 (Figure 5) represents an
338 austral summer dataset of *in situ* observations. Related confidence levels of the correlations can
339 be found in Table 3. For both time series, the SW product performed poorly across all wind
340 speed categories and the majority of the correlations fell outside of confidence intervals. The SW
341 product was observed to consistently have the highest error, especially so during high winds.
342 Overall the lowest error varies, but is shown by the ECMWF wind product during the CSIR2
343 time series (all wind speed RMSE = 2.62 m s^{-1}) and by the NCEPII product during the CSIR1
344 time series (all wind speed RMSE = 2.52 m s^{-1}). For the *all* wind speed and *medium* wind speed
345 categories, the ECMWF product had the highest correlation coefficients overall with respect to
346 the WG *in situ* data.

347 ECMWF exhibited the following correlation coefficients for the *all* wind speed category:
348 0.76 and 0.93, and the following coefficients for the medium wind speed category: 0.40 and 0.81
349 (Table 3). Low wind speeds are best represented overall by the CFSv2 product, with correlation
350 coefficients of 0.21 and 0.58, respectively. Statistically, the NCEPII product outperformed all
351 other products in the high wind speed category with coefficients of 0.74 and 0.82, even though it
352 significantly overestimated the magnitude of low and high winds during the CSIR2 time series
353 (Figure 4). This overestimation positively skews the overall correlation of the NCEPII with the
354 *in situ* data, which would suggest that it is not best suited to represent the temporal variability of
355 this particular time series even though the statistics in Table 3 would suggest otherwise.

Therefore, the CFSv2 and ECMWF products similarly best represent the high wind speed category and in general best represent the temporal variability of the wind field during this sampling period.

The bias exhibited by all wind products with respect to the data collected by the WG ranged from as small as -0.18 m s^{-1} (CFSv2 vs CSIR2 – 2015 *all* wind speed category) to as large as -9.23 m s^{-1} (SW vs CSIR1 2015-2016 *high* wind speed category). Similar to the RMSE, the trends in bias are different during each time series. During the CSIR2 time series (July – November 2015) the bias for the ECMWF, CFSv2, and NCEPII products remained fairly consistent across wind speed categories, but exhibited a positive bias for low winds and a negative bias for medium and high winds (exception- NCEPII high winds). The SW product during this time series exhibited a highly positive bias of +3.14 m s^{-1} for the low speed category, -0.49 m s^{-1} for the medium wind speed category, and -3.80 m s^{-1} for the high wind speed category. This trend in bias was only exhibited by the SW and ECWMF products during the CSIR2 time series (July – November 2015) and causes the SW product to appear better in performance than the NCEPII product in this respect (SW *all* wind speed bias = -0.42 m s^{-1}, NCEPII *all* wind speed bias = +1.13 m s^{-1}). During the CSIR1 time series (December 2015-February 2016) all products exhibited a systematic increase in bias with an increase in wind speed; however, the magnitude of increase was largest for the SW and smallest for the NCEPII product. Additionally, during this time series, all products exhibited a negative bias, indicative of an underrepresentation of the measured wind field (exception- SW *low* wind speed category).

Figure 6 visualizes the wind speed residuals from the wind products. There is an observed offset between the linear fit for each time series across all wind products; the CSIR2 time series exhibits residuals on average 2 m s^{-1} higher than the CSIR1 time series. The SW

product is observed to consistently overestimate low wind speeds, and significantly underestimate high wind speeds. The ECMWF and CFSv2 products exhibit very similar trends in residuals and only slightly overestimate low wind speeds and slightly underestimate high wind speeds. The NCEPII product performs differently per time series by having the smallest residuals at highest wind speeds during the CSIR2 time series, and the largest residuals at highest wind speeds during the CSIR1 time series. Although each product performs slightly different from one another, they all follow the same trend: overestimating low wind speeds, and underestimating high wind speeds.

To assess which of the wind products offers a characterization of the WG wind regime closest to reality, a Weibull PDF is used (Figure 7). For the CSIR2 time series (July 2015 - November 2015), the ECMWF product wind speed frequency distribution is almost identical to the WG frequency distribution, with the CFSv2 product being a close second. The SW product exhibits a similar curve but significantly overestimates the frequency of the medium wind speeds while underestimating frequencies of high wind speeds. The NCEPII product underestimates the frequencies of low and medium wind speeds and overestimates the frequencies of high wind speeds during austral spring. However, during the CSIR1 time series (December 2015 - February 2016), the NCEPII product best represents the frequency distribution of the *in situ* wind speeds. During austral summer the SW, ECMWF, and CFSv2 products overestimate the frequency of low and medium wind speeds, and underestimate the frequency of high wind speeds. While the *in situ* wind speed frequency distribution varies between the two time series, the products consistently estimate similar frequency distributions. This could be a result of sensor calibration offsets between the Airmar sensors and/or a seasonal change in the wind distributions between the two time series. When compared to the other products, the SW product systematically

represented the wind fields having higher frequencies of lower wind speeds. The ECMWF and CFSv2 products are characterized by a more even frequency distribution across all wind speed categories, while the NCEPII product tended to introduce reduced variability in the wind speed frequency distribution. It was observed that the higher the maximum wind speed of the wind product, the greater the variability and the more even the distribution of wind speeds.

4. Discussion

4.1 Comparing field data to global wind products

At global scale, numerous gridded scatterometer and/or reanalysis wind products such as QuikSCAT, Oceansat-2 Scatterometer (OSCAT) and Cross-Calibrated Multi-Platform (CCMP), tend to overestimate the true wind speed exponentially with respect to wind intensity (Carvalho et al., 2013), and have the highest margins of error during low and high wind events (Sudha et al., 2013; Alvarez et al., 2014; Jayaram et al., 2014). However, because various wind products have not been rigorously inter-calibrated, any comparison between satellite- and model derived wind data- with *in situ* data will only give relative information on accuracy (Vogelzang et al., 2012).

Based on our results, the performance of each product varied with respect to time of year and wind strength. The SW product consistently underestimated the wind fields and exhibited poor correlation across all wind speeds. As such it is not considered the preferred wind product for use in process understanding of upper ocean dynamics or realistic numerical analysis in the Southern Ocean. This may, in part be attributed to the fact that while SW data are available at a relatively high spatial resolution (0.25° x 0.25°), it is a gridded satellite product. This product

uses a simple objective analysis method (spatial-temporally weighted interpolation) to generate a gridded and blended product (Zhang, 2006). This method of blending satellite observations minimizes but does not completely eliminate data gaps. As such, the high resolution of spatial and temporal sampling conducted by WG technology may not be represented accurately by the SW dataset. There is a dearth of in situ observations in this remote ocean, which leads to difficulties in validation of any given wind product. This is further amplified by our poor understanding of the surface boundary layer, where accurate estimates of both momentum and heat fluxes are poor and likely contribute to inaccurate algorithms and bulk formulas that are used to derive satellite wind estimates (Gille et al., 2016). Furthermore, such a gap in observational input may lead to inadequate assimilation and parametrization of the boundary layer and surface frictional processes. This can ultimately impact how we derive and model (reanalyse) wind estimates to produce gridded wind products. SW also poorly represent wind estimates at different wind speed thresholds, particularly at high wind states. This indicates that there may be issues with how satellite scatterometer data is interpreted during extreme events which could be a result of high sea state (swell), surface wave breaking and surface turbulence all affecting the backscatter observed by the satellite. The strong performance of all reanalysis wind products in this study is indicative of improved algorithms and model parameterisations for different wind speeds related to different sea states. The improved performance of both the ECMWF and CFSv2 products may be attributed to the high spatial resolution of the datasets (0.125° x 0.125°, and 0.205° x 0.204° respectively) that take into account finer scale variability in the wind field and meteorological processes. In this study, four of the ECMWF sampling locations fall either directly on or within a tenth of a degree (~10 km) away from the circumference of the octagon sampling pattern (Figure 2) of the WGs for both time series. For

447 the NCEPII product, the nearest point of reference to the majority of the *in situ* measurements is
448 roughly 100 km (see Figure 2). Such low resolution data could lead to larger uncertainties
449 between NCEPII and the *in situ* measurements. Overall, the ECMWF product performs best
450 (with *all* wind speed correlations of 0.76 and 0.93) at consistently representing the temporal wind
451 field variability as observed by the WG.

452 During the CSIR2 time series (July 2015 – November 2015), measures of error and bias
453 for ECMWF and CFSv2 were lower than for NCEPII for all wind speed categories. However,
454 during the CSIR1 time series (December 2015- February 2016) the NCEPII product outperforms
455 all other products with regard to error and bias. While the CFSv2 product is better than ECMWF
456 at representing the mean wind state of low and medium wind speeds, ECMWF is better at
457 representing the temporal variability of the wind field magnitude. Upon closer inspection of the
458 performance of the NCEPII product, it best represented the mean wind state by exhibiting similar
459 trends in standard deviation across wind speed categories. For example, across time series the
460 NCEPII product had similar deviations from the mean of the low and medium wind speed
461 categories, and a greater deviation for the high wind speed category. This trend is also depicted
462 by the *in situ* data (Table 2); however, all other products exhibit opposing trends in deviation
463 from the mean. Due to these factors, the NCEPII product is best at representing the mean wind
464 state and deviation from the mean state, particularly during periods of high wind speeds.
465 However, this product should be used with caution, given that NCEPII derives its overall high
466 correlation through its overestimation of low and high wind speeds (Figure 6).

467 The ability of a product to best represent the wind speed frequency distribution is
468 illustrated in Figure 7. Findings by Pickett et al. (2003) and Tang et al. (2004) suggest that
469 satellites measure higher frequencies of strong winds and lower frequencies of weak winds.

However, during this study the frequency distribution of the *in situ* wind speeds varied between times series, while the frequency distribution of the satellite product wind speeds remains consistent. As such, a different product for each time series best represented the frequency distribution of observed wind speeds (Figure 7). The SW product consistently showed higher frequencies of low wind speeds which did not reflect the frequency distribution of the *in situ* winds for either time series. ECMWF and CFSv2 similarly showed a more uniform distribution of wind speed frequencies which almost perfectly matched the frequency distribution measured by the CSIR2 WG during the July – November 2015 time series. There was an observed 2.52 m s^{-1} increase in the mean wind speed of the CSIR1 time series (December 2015 – February 2016) with respect to the CSIR2 time series (Table 2). NCEPII consistently showed a broader distribution of speed frequencies, and thus this product best represented the frequency distribution of wind speeds during the CSIR1 time series.

Satellite derived wind data as well as reanalysis and model products can be very different from in-situ anemometer data in that they tend to represent synoptic-scale wind perturbations. A study by Atlas et al. (1999) showed that satellite products can detect mesoscale features, however this representation is limited since satellite and NWP products are of lower spatial and temporal resolution (Carvalho et al., 2013). Anemometer wind data is closer to a temporal average of instantaneous moments, while satellite winds represent a spatial average of instantaneous moments (Pansieri et al., 2010). Studies have shown that in cases where a limited amount of data existed, such as from a single satellite, any interpolations or extrapolations were inaccurate in representing the true strength of mesoscale events (Isaksen and Stoffelen, 2000). Bearing this in mind, over most SW grids the number of observational input data points is over 40 (Zhang, 2006). As such a multiple satellite blending scheme can be advantageous in representing fine

493 scale wind perturbations in the Southern Ocean. ECMWF, on the other hand, is a reanalysis
494 product using a sequential data assimilation scheme, advancing forward in time using 12 hourly
495 analysis cycles (Dee et al., 2011). A temporally short-scale assimilation scheme could give
496 ECMWF an advantage over other reanalysis products, such as NCEPII, in representing the
497 temporal variability on shorter temporal scales, as is a dominant scale of this study. CFSv2 is a
498 fully coupled ocean–land–atmosphere dynamical model using a global ocean data assimilation
499 system (GODAS) operational at NCEP (Saha et al., 2014). This product is unique in that it
500 makes retrospective forecasts to calibrate operational subsequent real time sub-seasonal and
501 seasonal predictions (Saha et al., 2014). This calibration scheme could be why CFSv2 is a more
502 rounded product and performs well in representing both the temporal variability and the mean
503 wind state. The NCEPII product is also a model simulation (forecast/hindcast reanalysis);
504 however, the data assimilation scheme is slightly different to ECMWF which is forced to
505 conform to observational input. Using 4-D data assimilation methodology, observational input
506 from ships, satellite, radiosonde, aircraft, and meteorological station observations are
507 incorporated into NCEPII (Kalnay et al., 1996). An assimilation methodology with high input
508 gives NCEPII the ability to represent regional climate dynamics (Kanamitsu et al., 2002), even
509 though it is of the coarsest spatial resolution compared to all other wind products.

510 ***4.2 Wave Glider meteorological sampling assumptions and potential shortcomings***

511 Compared to conventional *in situ* meteorological observing platforms, such as ships and
512 moorings, the WG has a low profile with respect to sea level with the Airmar sensor located just
513 0.7m above the sea surface. As stated in the methods, all wind observations in this study are
514 extrapolated to 10m above the sea surface for comparison to the wind products. However, this
515 proximity of sampling so close to the sea surface may not fully comprehend the impact of

surface friction and wave sheltering of the true wind field, especially in the case of extreme wind events or storms where large swell conditions of the Southern Ocean may impact the WG to product comparison. This scenario may explain the greater observed bias between the WG and product winds as a function of increasing wind speed and the impacts felt by the associated increase in sea state. This would suggest that wind observations from near surface platforms measure the winds between waves rather than the wind field 'above' the ocean surface. As such WGs are likely prone to underestimating wind speeds, particularly in the presence of large waves, and so are more suited to characterizing wind variability versus wind speed magnitude. In future deployments, ship-based meteorological observations could be used to compare with the WG observations to assess the magnitude and behavior of these potential inaccuracies in varying sea states and wind regimes. In addition, the Airmar sensor is prone to larger errors at higher wind speeds (see Methods section), which could contribute to the enhanced bias with higher wind speeds.

Furthermore, the WG measures absolute wind conditions at a particular location, while scatterometers measure wind relative to a moving ocean surface (Sudha and Rao, 2013). Dickinson et al. (2001) observed that during alignment (both in same and opposite direction) of both wind and surface ocean current, scatterometer data tend to be under or overestimated. This could partially explain the bias observed by products using scatterometer data. Shown in Table 2, the greatest standard deviation of wind products is often associated with low wind speeds (except for NCEPII), potentially indicative of the scatterometer inability to appropriately detect weak wind speeds due to the limited detection limits of the sensor in measuring surface scatter caused by wind-surface interaction. Additionally, the relation between wind and backscatter is provided by an empirical geophysical model function. However, because the quantity of backscatter

cannot be obtained during *in situ* sampling, model functions have varying methods of interpretation and subsequent assumptions which may not translate as intended for remote locations such as the Southern Ocean. An example of such an assumption is of the neutral stratification of the marine atmospheric boundary layer which is on average weakly unstable and the global average neutral equivalent wind is ~0.2 m s^{-1} stronger than real wind (Hersbach, 2009). Ebuchi et al. (2002) note the generation of small-scale waves via wind stress also varies with respect to atmospheric stability, which in turn affects radar backscatter used to derive wind speed. In addition, the difference between surface air temperature and SST is largely responsible for variability in stability. In the condition of a stable boundary layer, neutral equivalent winds can be lower than real winds by as much as 0.5 m s^{-1} (Hersbach, 2009). A similar argument can be made for the WG where in this study the vertical transformation of WG data did not include information on the atmospheric stability because we have no observations of the relative humidity from the WG. It is possible that data transformation could be in the order of 0.7 m s^{-1} greater in magnitude (Singh et al., 2013). In future deployments and glider experiments, the measurement of the atmospheric stability via relative humidity - not yet available on sensors located in such proximity to the sea surface - should be included in order to reduce uncertainty in the WG derived winds.

4.3 Broader implications

Ocean circulation modelling, climate change estimation, and numerical weather predictions are heavily dependent on the accuracy of input of meteorological information. Upper ocean dynamics are closely linked to atmospheric variability, particularly in the Southern Ocean where wind magnitudes and heat flux variations are great. As mentioned previously, the mid-latitude regions of the Southern Ocean are host to the strongest wind fields at the ocean surface.

If these winds are not accurately represented, models will incorrectly simulate a range of processes and parameters such as air-sea exchanges of heat and moisture, lateral advection, stratification and mixed layer dynamics (frontal formation and instabilities), Ekman pumping and transport. Given the importance of this, the present study and others shows that in many cases the wind fields are poorly represented.

Upper ocean models which include satellite-derived wind speed input do not accurately represent variance in mixed layer depth (MLD) and SST. Ocean circulation models have shown the sensitivity of the MLD to the gustiness in the wind (Lee et al., 2008). Turbulent mixing and subsequent buoyancy forcing caused by sea surface winds strongly influences the MLD. As the MLD shallows, high wind events are observed to have a greater impact on the deepening of the mixed layer (Carranza and Gille, 2015). Carranza and Gille (2015) observed that during high wind events, water from below the mixed layer is entrained in the upper ocean as the mixed layer deepens. Swart et al. (2015) observe with high-resolution glider datasets that this variability of the MLD is driven by synoptic storms (4-9 days) where turbulent mixing deepens the surface mixed layer, while quiescent wind episodes allow the upper ocean to restratify and subsequently shoal the MLD (du Plessis et al, 2017). This wind-driven mixing also influences SST, where cold water from below the MLD is entrained in the upper ocean. This in turn influences the mixed layer heat budget (Bonekamp et al., 1999) and produces cooler SSTs. Carranza and Gille (2015) found a statistically significant negative correlation between wind speed and SST anomalies, and that wind speed alone can explain as much as 80% of the variance observed in SSTs. The accurate representation of these upper ocean dynamics has been proven to have important implications for numerous chemical, biogeochemical and biological processes (e.g. Thomalla et

584 al., 2011; Fauchereau et al., 2011; Swart et al., 2015; Carranza and Gille 2015), as well as
585 biogeochemical models (e.g. Nicholson et al., 2016), that are not elaborated on in this study.
586

587 **5. Conclusion**

588 Predictions of heat, moisture, and momentum exchanges between the ocean and the
589 atmosphere remain uncertain in data sparse regions, such as the Southern Ocean (Gille et al.,
590 2016). We use high-frequency observations of wind stress obtained from WG deployments in the
591 Subantarctic Ocean to compare with four available satellite scatterometer and reanalysis global
592 wind products. It was found that the NCEPII product best represented the mean wind state in
593 certain conditions, namely with respect to the high wind speed category correlations for both
594 time series (0.74 and 0.82, respectively). Overall, ECMWF most consistently represented the
595 temporal wind field variability as observed by the glider, by representing the highest 'all' wind
596 speed correlations with coefficients of 0.76 and 0.93 for the independent time series. CFSv2 was
597 a close performer to ECMWF in its representation of the temporal wind field variability with
598 correlations differing on average < 0.05 from the ECMWF correlations with the WG. However,
599 on average CFSv2 had a slightly higher bias and RMSE (on average < 0.2 m s^{-1}) compared to
600 ECMWF. The results clearly showed that the SW product performed poorly at representing the
601 mean or wind stress variability (majority of the correlations <0.1) compared to those observed by
602 the WG.

603 The overall comparison between WG winds and gridded products in this study provide
604 confidence that autonomous surface vehicles, such as the WG, can be used to understand and
605 validate satellite-derived wind estimates. Further use of such vehicles should be supported to
606 provide improved time and space scale data sets and data volumes, particularly in remote and

607 harsh regions, such as the high-latitude oceans. There is a need to correctly parameterize
608 transient and synoptic scale wind fields in order to improve depictions of decadal and century
609 scale changes in ocean-atmosphere relationships.

610

ACKNOWLEDGEMENTS

The Wave Glider wind data were provided by the Southern Ocean Carbon & Climate Observatory, Council for Science and Industrial Research (CSIR). The authors of this work would like to thank SANAP and the captain and crew of the *S.A. Agulhas I* and *S.A. Agulhas II* for their contribution in the deployment and retrieval of the Wave Gliders. We acknowledge the work of SAMERC – Sea Technology Services for housing, managing, and piloting the gliders. The South African ocean glider program is supported by the Department of Science & Technology (DST) through the Sustainability & Innovation in Southern Ocean Observational Infrastructure grant. The SeaWinds blended altimetry data, CFS climate forecast, and NCEPII reanalysis wind product was downloaded from NOAA's National Centers for Environmental Information (NOAA/NCDC). The ECMWF reanalysis wind product was downloaded from the European Centre for Medium-Range Weather Forecasts open access database. The authors also thank two anonymous reviewers of K. Schmidt's MSc. dissertation, which has been used to present this study, as well as two anonymous reviewers of this paper. S. Swart thanks the following funding agencies: South African National Research Foundation (NRF) – grant SNA14071475720; and a Wallenberg Academy Fellowship.

633 **REFERENCES**

634 Alvarez, I., Gomez-Gesteira, M., deCastro, M., Carvalho, D., 2014. Comparison of different wind
635 products and buoy wind data with seasonality and interannual climate variability in the southern Bay
636 of Biscay (2000–2009). Deep-Sea Res. II. 106, 38 - 48. DOI: 10.1016/ j.dsr2.2013.09.028.

637 Atlas, R., Bloom, S. C., Hoffman, R. N., Brin, E., Ardizzone, J., Terry, J., Bungato, D., Jusem, J. C.,
638 1999. Geophysical validation of NSCAT winds using atmospheric data and analyses. J. Geophys.
639 Res. 104(C5), 11405 - 11424. DOI: 10.1029/98JC02374.

640 Bentamy, A., Croize-Fillon, D., Perigaud C., 2008. Characterization of ASCAT measurements based on
641 buoy and QuikSCAT wind vector observations. Ocean Sci. 4, 265 - 274. DOI: 10.5194/os-4-265-
642 2008.

643 Bonekamp, H., Sterl, A., Komen, G. J., 1999. Interannual variability in the Southern Ocean from an
644 ocean model forced by European Centre for Medium-Range Weather Forecasts reanalysis fluxes. J.
645 Geophys. Res. 104(C6), 13317 - 13331. DOI: 10.1029/ 1999JC900052.

646 Bourassa, M. A., Vincent, D. G, Wood, W. L. 1999a. A flux parameterization including the effects of
647 capillary waves and sea state. J. Atmo. Sci. 56, 1123 - 1139.

648 Bourassa, M. A., Legler. D. M., O'Brien, J. J., Smith, S. R., 2003. SeaWinds validation with research
649 vessels. J. Geophys. Res. 108(C2), 2156 - 2202. DOI: 10.1029/ 2001JC001028.

650 Carranza, M. M., Gille, S. T., 2015. Southern Ocean wind-driven entrainment enhances satellite
651 chlorophyll-a through the summer. J. Geophys. Res. 120**,** 304 - 323. DOI: 10.1002/2014JC010203.

652 Carvalho, D., Rocha, A., Gomez-Gesteira, M., Alvarez, I., Silva Santos, C., 2013. Comparison between
653 CCMP, QuikSCAT and buoy winds along the Iberian Peninsula coast. Remote Sens. Environ. 137,
654 173 - 183. DOI: 10.1016/j.rse.2013.06.005.

Chelton, D. B., Schlax, M. G., Freilich, M. H., Milliff R. F., 2004. Satellite Measurements Reveal Persistent Small-Scale Features in Ocean Winds. Science. 303, 978 - 983. DOI: 10.1126/science.1091901.

Dee, D. P., Uppala, S. M., Simmons, A. J., Berrisford, P., Poli, P., Kobayashi, S., Andrae, U., Balmaseda, M. A., Balsamo, G., Bauer, P., Bechtold, P., Beljaars, A. C. M., van de Berg, L., Bidlot, J., Bormann, N., Delsol, C., Dragani, R., Fuentes, M., Geer, A. J., Haimberger, L., Healy, S. B., Hersbach, H., Hólm, E. V., Isaksen, L., Kållberg, P., Köhler, M., Matricardi, M., McNally, A. P., Monge-Sanz, B. M., Morcrette, J.-J., Park, B.-K., Peubey, C., de Rosnay, P., Tavolato, C., Thépaut, J.-N., Vitart, F., 2011. The ERA-Interim reanalysis: configuration and performance of the data assimilation system. Q.J.R. Meteorol. Soc., 137, 553 - 597. DOI:10.1002/qj.828.

Dickinson, S., Kelly, K. A., Caruso, M. J., McPhaden, M. J., 2001. Comparisons between the TAO buoy and NASA scatterometer wind vectors. J. Atmos. Oceanic Technol. 18, 799 - 806. DOI: 10.1175/1520-0426.

du Plessis, M., S. Swart, I. J. Ansorge, and A. Mahadevan, 2017. Submesoscale processes promote seasonal restratification in the Subantarctic Ocean. J. Geophys. Res. Oceans, 122. DOI: 10.1002/joc.5022.

Ebuchi, N., Graber, H. C., Caruso, M. J., 2002. Evaluation of Wind Vectors Observed by QuikSCAT/ Seawinds Using Ocean Buoy Data. J. Atmos. Oceanic Technol. 19:12, 2049 - 2062. DOI: 10.1175/1520-0426 (2002) 0192.0.

Fauchereau, N., Tagliabue, A., Bopp, L., Monteiro, P. M. S., 2011. The response of phytoplankton biomass to transient mixing events in the Southern Ocean. Geophys. Res. Lett. 38, L17601. DOI: 10.1029/2011GL048498.

677 Freilich, M.H., Vanhoff, B.A., 2002. The Relationship between Winds, Surface Roughness, and Radar
678 Backscatter at Incidence Angles from TRMM Precipitation Radar Measurements. J. Atmos. Oceanic
679 Technol. 20, 549-562.

680 Geleyn, JF. 1988. Interpolation of wind, temperature and humidity values from model levels to the
681 height of measurement. Tellus. 40A: 347–351.

682 Gille, S., Josey, S., Swart, S., 2016. New approaches for air-sea fluxes in the Southern Ocean, EOS, 97,
683 doi:10.1029/2016EO052243.

684 Herrera, J. L., Piedracoba, S., Varela, R. A., Roson, G., 2005. Spatial analysis of the wind field on the
685 western coast of Galicia (NW Spain) from *in situ* measurements. Cont. Shelf Res. 25, 1728 - 1748.
686 DOI: 10.1016/j.csr.2005.06.001.

687 Hersbach, H. 2009. Comparison of C-Band Scatterometer CMOD5.N Equivalent Neutral Winds with
688 ECMWF. J. Atmos. Oceanic Technol. 27. 721-736. DOI: 10.1175/2009JTECHO698.1.

689 Hilburn, K.A., Bourassa, M.A., O'Brien, J.J., 2003. Development of scatterometer-derived surface
690 pressures for the Southern Ocean. J. Geophys. Res. 108(C7), 32 - 44. DOI: 10.1029/2003JC001772.

691 Ho, D. T., Law, C. S., Smith, M. J., Schlosser, P., Harvey, M., Hill, P., 2006. Measurements of air-sea
692 gas exchange at high wind speeds in the Southern Ocean: Implications for global parameterizations.
693 Geophys. Res. Lett. 33, L16611. DOI:10.1029/2006GL026817.

694 Hu, Yongxiang., 2009. Ocean, Land and Meteorology Studies Using Space-Based Lidar Measurements.
695 5th WSEAS Int. Conf. on Remote Sensing. 2008, Genova, Italy. NASA Langley Research Center.
696 LF99-9425, Paper-626-301.

697 Isaksen, L., Stoffelen A., 2000. ERS-Scatterometer wind data impact on ECMWF's tropical cyclone
698 forecasts. IEEE Trans. Geosci. Remote Sens. 38, 1885 - 1892. DOI: 10.1109/36.851771.

699 Jayaram, C., Udaya-Bhaskar, T., Swain, D., Pattabhi, E., Rao, R., Bansal, S., Dutta, D., Hanumantha
700 Rao, K., 2014. Daily composite wind fields from Oceansat-2 scatterometer. Remote Sens. Lett. 5(3),
701 258 - 267. DOI: 10.1080/2150704X.2014.898191.

702 Kalnay, E., Kanamitsu, M., Kistler, R., Collins, W., Deaven, D., Gandin, L., Iredell, M., Saha, S., White,
703 G., Woollen, J., Zhu, Y., Leetmaa, A., Reynolds, R., Chelliah, M., Ebisuzaki, W., Higgins, W.,
704 Janowiak, J., Mo, K. C., Ropelewski, C., Wang, J., Jenne, R., Joseph, D., 1996. The NCEP/NCAR
705 40-year reanalysis project. Bull. Am. Meteorol. Soc. 77, 437 - 470. DOI: 10.1175/1520-0477.

706 Kanamitsu, M., Ebisuzaki, W., Woollen, J., Yang, S. K., Hnilo, J. J., Fiorino, M., Potter, L., 2002.
707 NCEP-DOE AMIP-II Reanalysis (R-2). Bull. Am. Meteorol. Soc. 83, 1631 - 1643. DOI:
708 10.1175/BAMS-83-11-1631.

709 Lee, T., Wang, O., Tang, W., Liu, W. T., 2008. Wind stress measurements from the QuikSCAT-
710 SeaWinds scatterometer tandem mission and the impact on an ocean model. J. Geophys. Res. 113,
711 C12019. DOI:10.1029/2008JC004855.

712 Liu, W. T., Tang, W., 1996. Equivalent Neutral Wind. Jet Propulsion Laboratory Publication 96-17.

713 Liu, W.T., Tang, W., Xie, X., 2008. Wind power distribution over the ocean. Geophys. Res. Lett. 35,
714 L13808. DOI: 10.1029/2008GL034172.

715 Mears, C. A., Smith, D. K., Wentz, F. J., 2001. Comparison of Special Sensor Microwave Imager and
716 buoy-measured wind speeds from 1987 to 1997. J. Geophys. Res. 106(11), 719 - 729. DOI:
717 1999JC000097.0148-0227/01/1999JC000097.

718 Monteiro, P. M. S., Gregor, L., Lévy, M., Maenner, S., Sabine, C. L., Swart, S., 2015. Intraseasonal
719 variability linked to sampling alias in air-sea CO_2 fluxes in the Southern Ocean. Geophys. Res. Lett.
720 42, 8507 – 8514. DOI: 10.1002/2015GL066009.

721 Nicholson, S. A., Lévy, M., Llort, J., Swart, S., Monteiro, P. M. S., 2016. Investigation into the impact
722 of storms on sustaining summer primary productivity in the Sub- Antarctic Ocean. Geophys. Res.
723 Lett. 43, 9192 - 9199. DOI: 10.1002/2016GL069973.

724 Nightingale, P.D., Malin, G., Law, C.S., Watson, A.J., Liss, P.S., Liddicoat, M.I., Boutin, J., Upstill-
725 Goddard, R.C., 2000. *In situ* evaluation of air-sea gas exchange parameterizations using novel
726 conservative and volatile tracers. Global Biogeochem. Cycles, 14(1), 373 - 387. DOI:
727 10.1029/1999GB900091.

728 Patoux, J., Yuan, X., Li, C., 2009. Satellite-based midlatitude cyclone statistics over the Southern Ocean:
729 1. Scatterometer-derived pressure fields and storm tracking. J. Geophys. Res. 114, D04105. DOI:
730 10.1029/2008JD010873.

731 Pickett, M. H., Tang, W., Rosenfeld, L. K., Wash, C. H., 2003. QuikSCAT satellite comparisons with
732 nearshore buoy wind data off the U.S. West Coast. J. Atmos. Oceanic Technol. 20, 1869 - 1979.

733 Qing, W.U., Chen, G., 2015. Validation and intercomparison of HY-2A/ MetOp-A/ Oceansat-2
734 scatterometer wind products. Chin. J. Oceanol. Limn. 33(5), 1181 - 1190. DOI:
735 10.1080/07055900.2013.869191.

736 Risien, C. M., Chelton, D.B. 2008. A Global Climatology of Surface Wind and Wind Stress Fields from
737 Eight Years of QuikSCAT Scatterometer Data. J. Phys. Oceanography. 38. 2379- 2413. DOI:
738 10.1175/2008JPO3881.1.

739 Ruti, P. M., Marullo, S., D'Ortenzio, F., Tremant, M., 2008. Comparison of analyzed and measured wind
740 speeds in the perspective of oceanic simulations over the Mediterranean basin: Analyses, QuikSCAT
741 and buoy data. J. Marine. Syst. 70, 33 - 48. DOI: 10.1016/j.jmarsys.2007.02.026.

742 Saha, S., Moorthi, S., Wu, X., Wang, J. et al., 2014. The NCEP Climate Forecast System Version 2. J.
743 Climate. 27, 2185 - 2208. DOI:10.1175/JCLI-D-12-00823.1.

744 Satheesan, K., Sarkar, A., Parekh, A., Kumar, M. R. R., Kuroda, Y., 2007. Comparison of Wind Data
745 from QuikSCAT and Buoys in the Indian Ocean. Int. J. Remote Sens. 28(10), 2375 - 2382. DOI:
746 10.1080/01431160701236803.

747 Singh, P., Parekh, A., Attada, R., 2013. Comparison of a single logarithmic and equivalent neutral wind
748 approaches for converting buoy-measured wind speed to the standard height: special emphasis to
749 North Indian Ocean. Theor. Appl. Climatol. 111, 455 - 463. DOI: 10.1007/s00704-012-0674-2.

750 Sudha, A.K., Prasada Rao, C.V., 2013. Comparison of Oceansat-2 scatterometer winds with buoy
751 observations over the Indian Ocean and the Pacific Ocean. Remote Sens. Lett. 4(2), 171 - 179. DOI:
752 10.1080/2150704X.2012.713140.

753 Swart, S., S. Speich, I. J. Ansorge, and J. R. E. Lutjeharms, 2010. An altimetry-based gravest empirical
754 mode south of Africa: 1. Development and validation, J. Geophys. Res., 115, C03002,
755 doi:10.1029/2009JC005299.

756 Swart, S., Chang, N., Fauchereau, N., Joubert, W., Lucas, M., Mtshali, T., Roychoudhury, A., Tagliabue,
757 A., Thomalla, S., Waldron, H., Monteiro, P.M.S., 2012. Southern Ocean seasonal cycle experiment
758 2012: seasonal scale climate and carbon links. S. Afr. J. Sci. 108(3/4), 1 - 3. DOI:
759 10.4102/sajs.v108i3/4.1089.

760 Swart, S., Thomalla, S.J., Monteiro, P.M.S., 2014. The seasonal cycle of mixed layer dynamics and
761 phytoplankton biomass in the Sub-Antarctic Zone: A high-resolution glider experiment. J. Marine
762 Syst. 147, 103 – 115. DOI: 10.1016/j.jmarsys.2014.06.002.

763 Tang, W., Liu, W. T., Stiles, B. W., 2004. Evaluation of High-Resolution Ocean Surface Vector Winds
764 Measured by QuikSCAT Scatterometer in Coastal Regions. IEEE Trans. Geosci. Remote Sens.
765 42(8), 1762 - 1769. DOI: 10.1109/ TGRS.2004. 831685.

766 Tardif, R., Laroche, S. 2012B. An equivalent neutral wind observation operator for variational
767 assimilation of scatterometer ocean surface wind data. Q.J.R. Meteorol. Soc. 138, 2086-2104.
768 DOI:10.1002/qj.1953.

769 Thomalla, S.J., Faucherau, N., Swart, S., Monteiro, P.M.S., 2011. Regional scale characteristics of the
770 seasonal cycle of chlorophyll in the Southern Ocean. Biogeosciences. 8, 2849 - 2866. DOI:
771 10.5194/bg-8-2849-2011.

772 Wanninkhof, R., 1992. Relationship between gas exchange and wind speed over the ocean. J. Geophys.
773 Res. 97(C5), 7373 - 7381. DOI: 92JC00188.0148-0227/92/92 J C-00188505.00.

774 Wanninkhof, R., McGillis, W. R., 1999. A cubic relationship between air-sea CO_2 exchange and wind
775 speed. Geophys. Res. Lett., 26(13), 1889 - 1892. DOI: 1999GL900363.0094-
776 8276/99/1999GL900363.

777 Wanninkhof, R., Asher, W. E., Ho, D. T., Sweeney, C., McGillis, W. R., 2009. Advances in Quantifying
778 Air-Sea Gas Exchange and Environmental Forcing. Annu. Rev. Mar. Sci., 1, 213 - 244. DOI:
779 10.1146/annurev.marine.010908.163742.

780 Yang, X., Liu, G., Li, Z., Yu, Y., 2014. Preliminary validation of ocean surface vector winds estimated
781 from China's HY-2A scatterometer. Int. J. Rem. Sens. 35(11-12), 4532 - 4543. DOI: 10.1080/
782 01431161.2014.916049.

783 Yuan, X., 2004. High-wind-speed evaluation in the Southern Ocean. J. Geophys. Res. 109, D13101.
784 DOI:10.1029/2003JD004179.

785 Yuan, X., Patoux, J., Li, C., 2009, Satellite-based midlatitude cyclone statistics over the Southern Ocean:
786 2. Tracks and surface fluxes. J. Geophys. Res. 114, D04106. DOI: 10.1029/ 2008JD010874.

787 Zhang, Huai-Min., 2006. Blended and Gridded High Resolution Global Sea Surface Winds from
788 Multiple Satellites. NOAA NESDIS National Climatic Data Center. 1 – 24.

Table and Figure captions:

Table 1: Characteristics of the different wind products used in this study

Table 2: The mean and standard deviation of all wind products and WG data per wind speed category, as defined in Section 2.3. All bold product values indicate the closest match to the WG data.

Table 3: Comparison between *in situ* WG and satellite/reanalysis products, which includes the wind speed error per wind speed category, root mean square error, bias, and correlation coefficients. The bold values highlight the wind product providing the closest match with the *in situ* data (i.e. the smallest value of error or bias and the highest value of the correlation coefficient). All correlation coefficients > |0.24| exhibit a confidence interval >99%. The number of comparative observations are shown by 'N'.

Figure 1. (a) The study region in the Subantarctic Ocean, with the main location of where the in situ data was collected at 43°00'S 8°30'0E (indicated by black square) and overlaid on the monthly averaged ECMWF wind speeds (m s^{-1}) for December 2015. The mean locations of the Southern Ocean fronts are overlaid (solid black curves) according to Swart et al., 2010. (b) The Liquid Robotics SV2 Wave Glider with the Airmar weather station indicated (photo credit: Fred Fourie).

Figure 2: Map of sampling region in the Southern Ocean, centered at 43°00'S 8°30'0E. The WG sampling locations, encompassing two separate deployments, are indicated with respect to spatial distribution of gridded wind products.

Figure 3: Comparison of wind products (colored curves) with *in situ* WG data (black line) and upper and lower limits of each product dotted lines of their respective colors. *(a)* WG CSIR2, July - November 2015. *(b)* WG CSIR1, December 2015 – February 2016. Data gaps in (a) represent periods when the meteorology sampling was stopped in order to save battery power during poor solar charging periods in winter-spring. SW represents the SeaWinds product.

Figure 4: Comparison of wind products with *in situ* (CSIR2 WG) data collected July 2015 – November 2015 (austral winter-spring). Wind speed categories are determined using the lower and upper quartiles of the *in situ* data. A linear fit for each wind speed category is shown.

Figure 5: Comparison of wind products with *in situ* (CSIR1 WG) data collected December 2015 – February 2016 (austral summer). Wind speed categories are determined using the lower and upper quartiles of the *in situ* data. A linear fit for each wind speed category is shown.

Figure 6: Wind speed residuals (wind product minus *in situ* data) for both WG time series. Linear fit for each time series and product is displayed in their respective colors.

832 **Figure 7:** Wind speed frequency distribution (Weibull PDF) for all products (SW, ECMWF,
833 CFSv2, and NCEPII) compared to *in situ* wind collection by Wave Gliders (a) CSIR2 and (b)
834 CSIR1.

835

836 **Tables and Figures:**

837

838 **Table 1:** Characteristics of the different wind products used in this study

Wind Products	Time (h) Resolution	Spatial Resolution	Reference	Time Coverage
SW	6	0.25° x 0.25°	*Zhang* 2006	09 July 1987 - Present
ECMWF	6	0.125° x 0.125°	*Dee et al.* 2011	1979 – 31 Jan 2016
CFSv2	6	0.205° x 0.204°	*Saha et al.* 2014	01 April 2011 - Present
NCEPII	6	1.875° x 1.904°	*Kanamitsu et al.* 2002	1979 - Present

839

840

841

842

843

844

845

846

847

848

849

Table 2: The mean and standard deviation of all wind products and WG data per wind speed category, as defined in Section 2.3. All bold product values indicate the closest match to the WG data.

TIME SERIES

CSIR2: July 2015 - Nov. 2015

CSIR1: Dec. 2015 - Feb. 2016

LOW WIND SPEEDS

CSIR2 ≤ 7.3 m s^{-1}

CSIR1 ≤ 9.0 m s^{-1}

MEDIUM WIND SPEEDS

7.3 m s^{-1} ≤ CSIR2 ≤ 12.4 m s^{-1}

9.0 m s^{-1} ≤ CSIR1 ≤ 16.0 m s^{-1}

HIGH WIND SPEEDS

CSIR2 ≥ 12.4 m s^{-1}

CSIR1 ≥ 16.0 m s^{-1}

	ALL (m s^{-1})	**LOW** (m s^{-1})	**MEDIUM** (m s^{-1})	**HIGH** (m s^{-1})
CSIR2	9.98 ± 3.76	5.21 ± 1.32	9.93 ± 1.46	14.83 ± 2.03
SW	9.63 ± 3.24	8.42 ± 3.06	9.51 ± 3.37	11.10 ± 2.49
CFSv2	**9.80 ± 3.97**	6.30 ± 3.04	**9.51 ± 2.86**	**13.86 ± 2.93**
ECMWF	9.58 ± 3.64	**6.25 ± 2.92**	9.39 ± 2.57	13.26 ± 2.57
NCEPII	11.11 ± 5.03	7.39 ± 3.81	10.52 ± 3.63	16.00 ± 4.70
CSIR1	12.50 ± 4.79	6.76 ± 1.84	12.20 ± 2.06	18.82 ± 2.53
SW	8.57 ± 3.14	7.36 ± 2.93	8.67 ± 3.14	9.59 ± 2.99
CFSv2	9.39 ± 4.05	5.17 ± 2.16	8.96 ± 2.39	14.50 ± 2.32
ECMWF	9.21 ± 3.90	4.95 ± 2.28	8.88 ± 2.16	14.12 ± 2.03
NCEPII	**11.15 ± 4.97**	**6.72 ± 2.70**	**10.67 ± 2.80**	**17.28 ± 3.41**

Table 3: Comparison between *in situ* WG and satellite/reanalysis products, which includes the wind speed error per wind speed category, root mean square error, bias, and correlation coefficients. The bold values highlight the wind product providing the closest match with the *in situ* data (i.e. the smallest value of error or bias and the highest value of the correlation coefficient). All correlation coefficients > |0.24| exhibit a confidence interval >99%. The number of comparative observations are shown by 'N'.

WG CSIR 1

Dec. 2015 - Feb. 2016

LOW WIND

WG ≤ 9.0 m s^{-1}

MEDIUM WIND

9.0 m s^{-1} ≤ WG; WG ≤ 16.0 m s^{-1}

HIGH WIND

WG ≥ 16.0 m s^{-1}

	CSIR1 vs:	ALL (m s^{-1})	LOW (m s^{-1})	MEDIUM (m s^{-1})	HIGH (m s^{-1})	N
RMSE	***SW***	6.37	3.23	5.24	9.84	243
	CFSv2	3.58	**2.39**	3.51	4.57	245
	ECMWF	3.70	2.43	3.42	5.06	217
	NCEPII	**2.52**	2.75	**2.40**	**2.50**	245
BIAS	***SW***	-3.92	**+0.60**	-3.53	-9.23	243
	CFSv2	-3.06	-1.55	-3.19	-4.32	245
	ECMWF	-3.16	-1.55	-3.16	-4.78	217
	NCEPII	**-1.31**	-0.75	**-1.47**	**-1.54**	245
R^2	***SW***	0.25	0.16	-0.08	0.24	243
	CFSv2	**0.93**	0.58	0.79	0.81	245
	ECMWF	**0.93**	**0.59**	**0.81**	0.77	217
	NCEPII	0.90	0.35	0.73	**0.82**	245

WG CSIR 2

July. 2015 - Nov. 2015

LOW WIND

WG ≤ 7.3 m s^{-1}

MEDIUM WIND

7.3 m s^{-1} ≤ WG; WG ≤ 12.4 m s^{-1}

HIGH WIND

WG ≥ 12.0 m s^{-1}

	CSIR2 vs:	ALL (m s^{-1})	LOW (m s^{-1})	MEDIUM (m s^{-1})	HIGH (m s^{-1})	N
RMSE	***SW***	4.25	4.58	3.64	4.95	250
	CFSv2	2.81	3.22	2.76	2.47	259
	ECMWF	**2.62**	**3.14**	**2.45**	**2.35**	259
	NCEPII	3.73	4.47	3.34	3.64	259
BIAS	***SW***	-0.42	+3.14	-0.49	-3.80	250
	CFSv2	**-0.18**	+1.09	**-0.43**	**-0.97**	259
	ECMWF	-0.40	**+1.04**	-0.54	-1.57	259
	NCEPII	+1.13	+2.18	-0.58	+1.17	259
R^2	***SW***	0.27	-0.03	0.05	0.01	250
	CFSv2	0.74	**0.21**	0.34	0.63	259
	ECMWF	**0.76**	0.17	0.40	0.73	259
	NCEPII	0.71	0.07	**0.42**	**0.74**	259

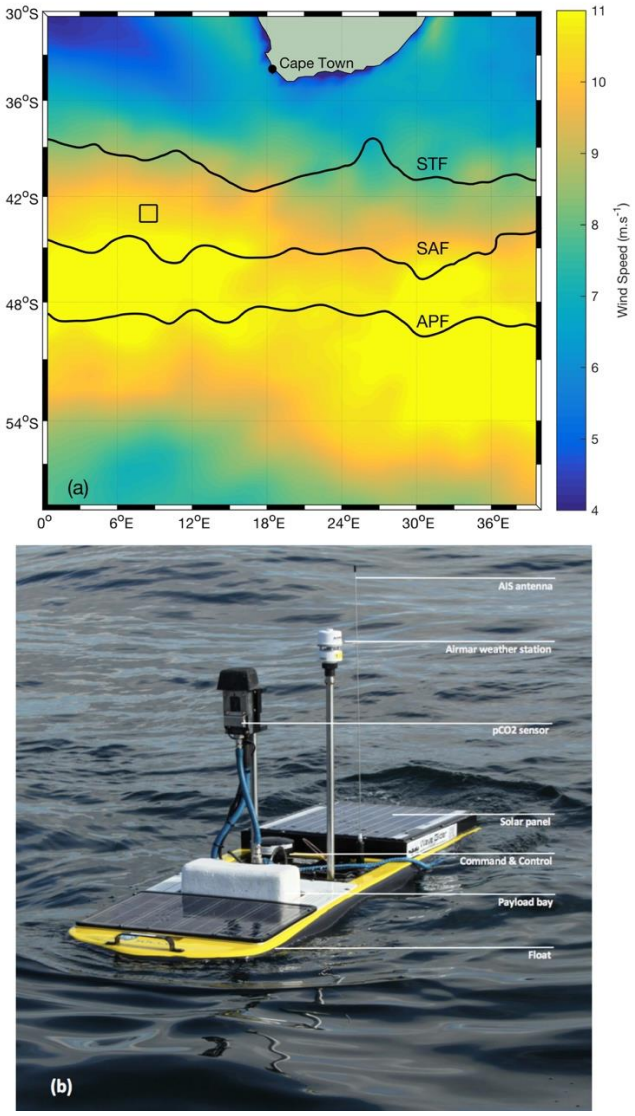

Figure 1. (a) The study region in the Subantarctic Ocean, with the main location of where the in situ data was collected at 43°00'S 8°30'0E (indicated by black square) and overlaid on the monthly averaged ECMWF wind speeds (m s^{-1}) for December 2015. The mean locations of the Southern Ocean fronts are overlaid (solid black curves) according to Swart et al., 2010. (b) The Liquid Robotics SV2 Wave Glider with the Airmar weather station indicated (photo credit: Fred Fourie).

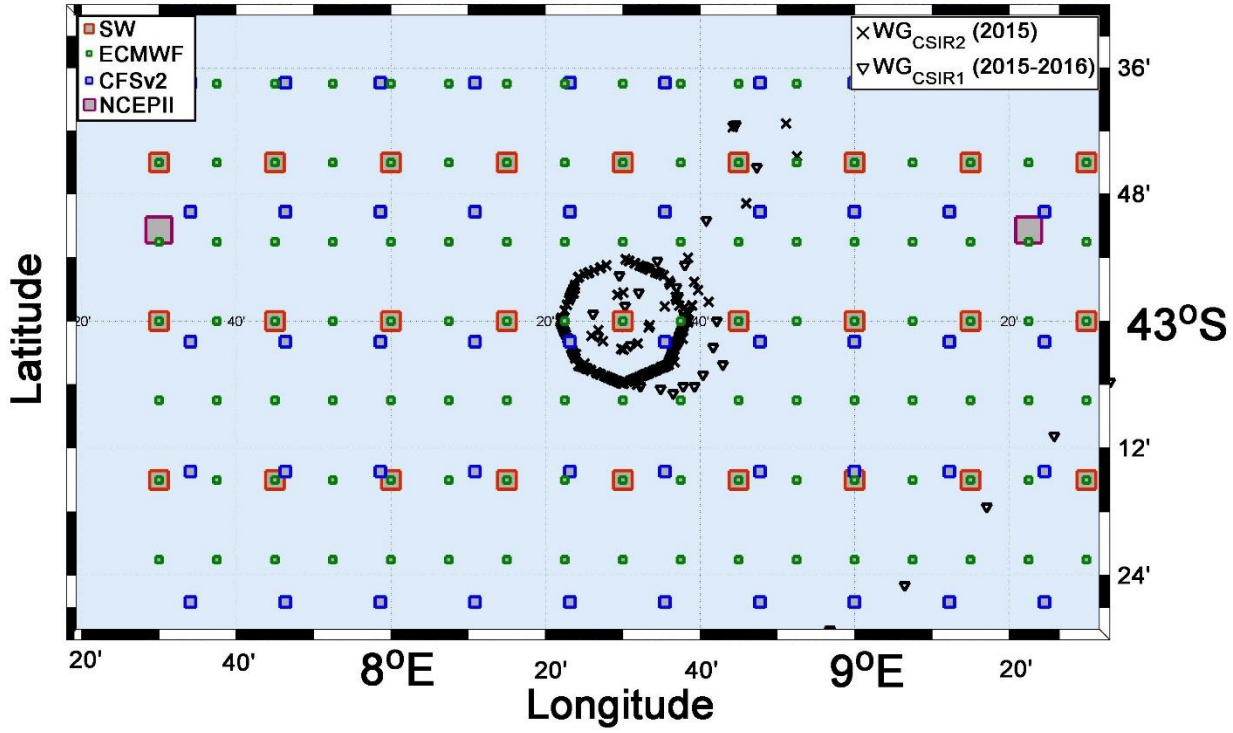

Figure 2: Map of sampling region in the Southern Ocean, centered at 43°00'S 8°30'0E. The WG sampling locations, encompassing two separate deployments, are indicated with respect to spatial distribution of gridded wind products.

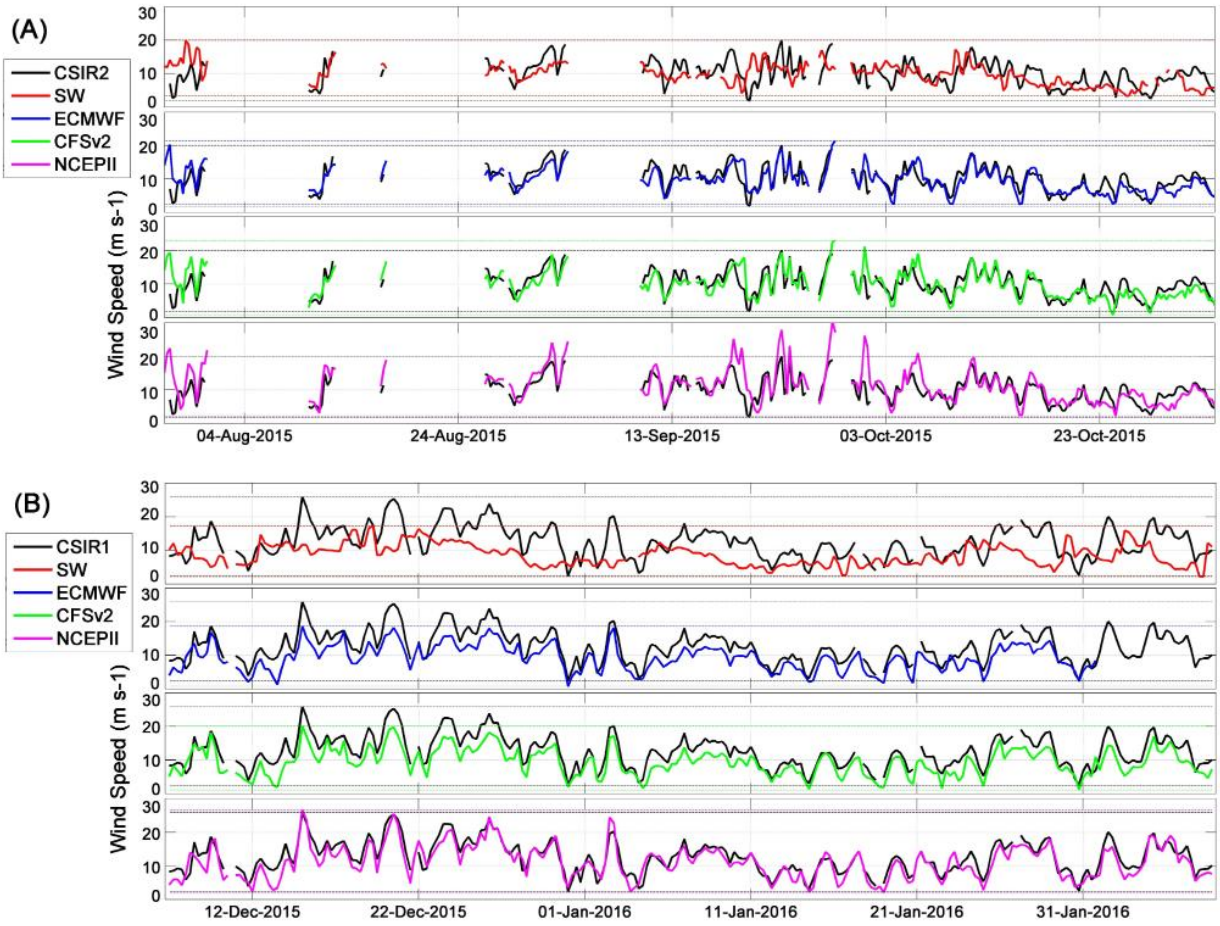

886

887 **Figure 3:** Comparison of wind products (colored curves) with *in situ* WG data (black line) and
888 upper and lower limits of each product dotted lines of their respective colors. *(a)* WG CSIR2,
889 July - November 2015. *(b)* WG CSIR1, December 2015 – February 2016. Data gaps in (a)
890 represent periods when the meteorology sampling was stopped in order to save battery power
891 during poor solar charging periods in winter-spring. SW represents the SeaWinds product.

892

893 .

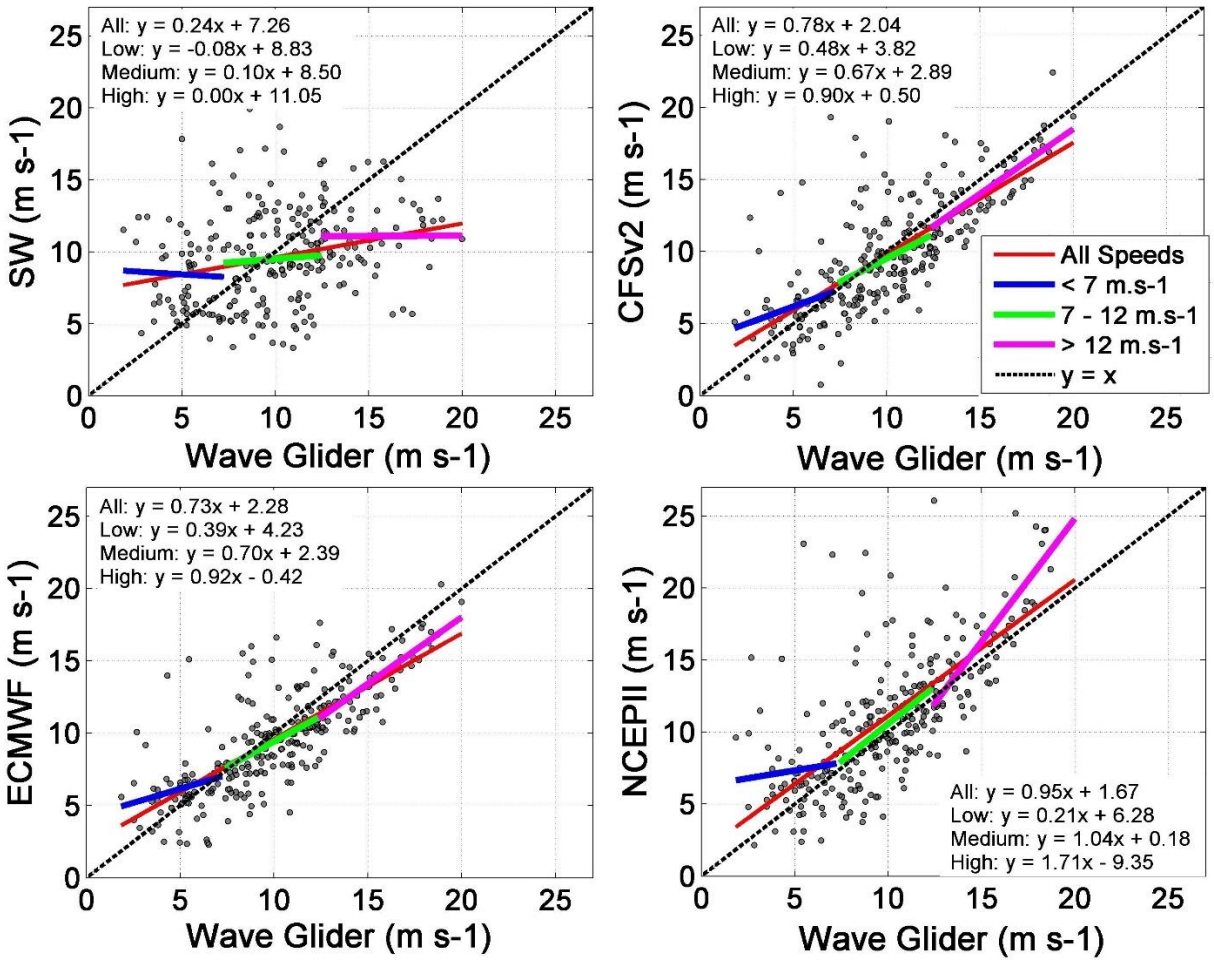

894

895 **Figure 4:** Comparison of wind products with *in situ* (CSIR2 WG) data collected July 2015 –
896 November 2015 (austral winter-spring). Wind speed categories are determined using the lower
897 and upper quartiles of the *in situ* data. A linear fit for each wind speed category is shown.

898

899

900

901

902

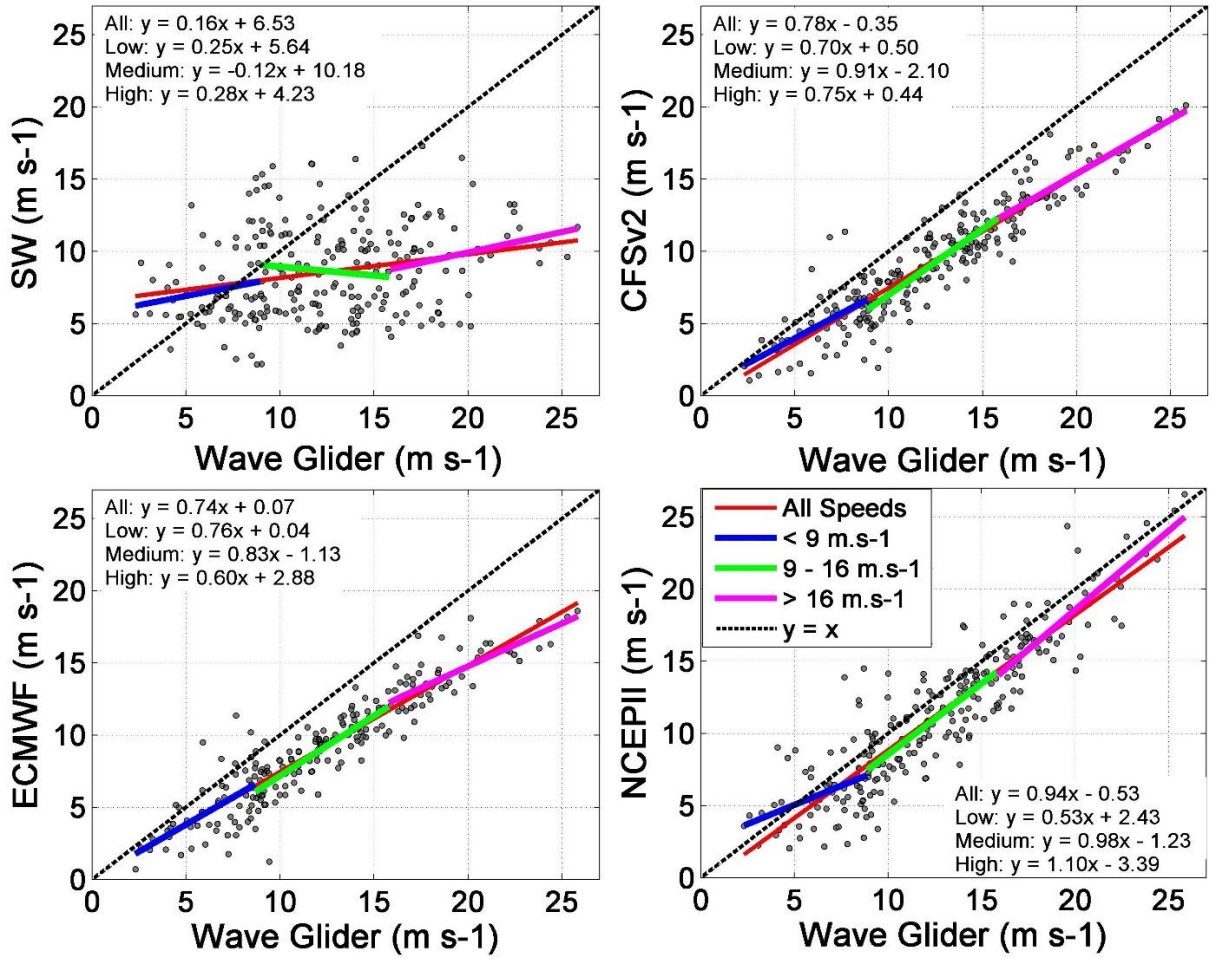

Figure 5: Comparison of wind products with *in situ* (CSIR1 WG) data collected December 2015 – February 2016 (austral summer). Wind speed categories are determined using the lower and upper quartiles of the *in situ* data. A linear fit for each wind speed category is shown.

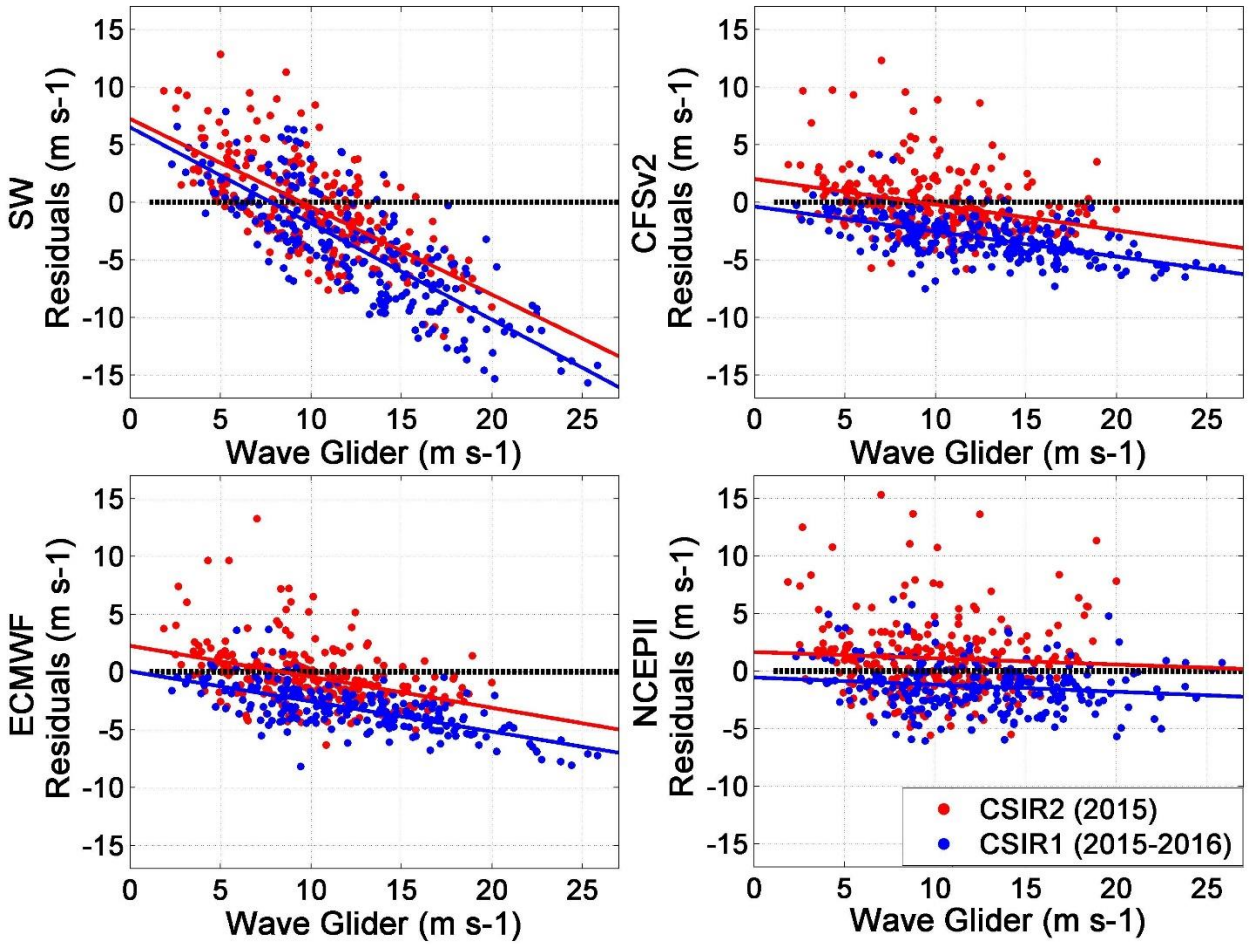

912

913 **Figure 6:** Wind speed residuals (wind product minus *in situ* data) for both WG time series.

914 Linear fit for each time series and product is displayed in their respective colors.

915

916

917

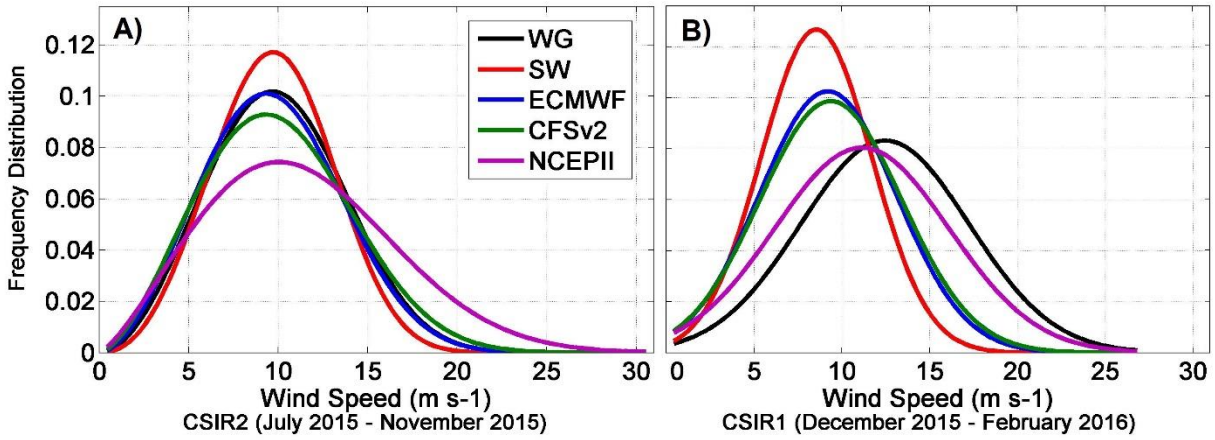

Figure 7: Wind speed frequency distribution (Weibull PDF) for all products (SW, ECMWF, CFSv2, and NCEPII) compared to *in situ* wind collection by Wave Gliders (a) CSIR2 and (b) CSIR1.